

Contents lists available at ScienceDirect

Journal of the Mechanical Behavior of Biomedical Materials

Journal of het Mechanical Behavior of Biomedical Materials

journal homepage: www.elsevier.com/locate/jmbbm



On the examination of the viscous response of the brachial artery during flow-mediated dilation

Bchara Sidnawi ^{a,b}, Sridhar Santhanam ^a, Chandra Sehgal ^c, Qianhong Wu ^{a,b,*}

- ^a Department of Mechanical Engineering, Villanova University, PA, 19085, USA
- ^b Cellular Biomechanics and Sport Science Laboratory, Villanova University, PA, 19085, USA
- ^c Department of Radiology, University of Pennsylvania, PA, 19104, USA

ARTICLE INFO

Keywords: Flow mediated dilation Fluid-structure interaction Mechanotransduction Wall shear stress Viscoelastic model

ABSTRACT

In this study, mechanotransduction is investigated through a physics-based viscoelastic model describing the arterial diameter response during a brachial artery flow mediated dilation (BAFMD) test. The study is a significant extension of two earlier studies by the same group, where only the elastic response was considered. Experimental BAFMD responses were collected from 12 healthy volunteers. The arterial wall's elastic and viscous properties were treated as local variable quantities depending on the wall shear stress (WSS) sensed by mechanotransduction. The dimensionless parameters, arising from the model which serve as a quantitative assessment of the artery's physical state, were adjusted to replicate the experimental response. Among those dimensionless parameters, the viscoelastic ratio, which reflects the relative strength of the viscous response compared to its elastic counterpart, is of special relevance to this paper's main conclusion. Based on the results, it is concluded that the arterial wall's mechanical behavior is predominantly elastic, at least in the strict context of the BAFMD test. Recommendations for potential future research and applications are provided.

1. Introduction

Flow Mediated Dilation (FMD), which is arteries' expansion in response to an increase in blood flow is one of the telltales of arterial integrity. A well-known, inexpensive, in-vivo, and noninvasive way to inspect this function is the brachial artery FMD (BAFMD) test. An individual undergoing the BAFMD test, has a pressure cuff wrapped around their upper arm and inflated for a duration that is enough to cut off the blood flow to the lower arm, and completely collapse the brachial artery as it is being monitored via an ultrasound scanner. The cuff is then deflated, and the artery's recovery to its baseline diameter is observed. An illustration of the test is shown in Fig. 1.

Suboptimal FMD has been linked to many underlying cardiovascular health problems and risk factors (Stoner et al., 2004; Celermajer et al., 1993; Nakamura et al., 2011; Hashimoto et al., 1998; McCully, 2012; Birk et al., 2012; Pyke and Tschakovsky, 2005; Kaź mierski et al., 2010). Furthermore, a recent experimental study has shown a much-improved correlation between acetylcholine-induced coronary vascular function and the brachial artery's FMD (Broxterman et al., 2019) Therefore, a rigorous understanding of the mechanisms driving the observed artery's behavior after cuff deflation could offer valuable insights into a subject's

overall arterial health, and through regular monitoring, early transpiring signs of emerging problems could prop up treatments' prospect of success.

The primary progenitor of FMD is mechanotransduction, through which mechanical cues such as blood pressure and wall shear stress originating in the flow environment are relayed to the arterial wall's internal structure which then responds accordingly to accommodate changing flow conditions by changing the arterial compliance. Mechanotransduction requires a functional Endothelial Glycocalyx Layer (EGL), a negatively charged soft, porous layer lining the arterial wall's inner surface (Weinbaum et al., 2003, 2007). Upon sensing a change in flow conditions, the EGL mechanically transmits the signal to the Endothelial Cells (ECs) surface, thereby initiating a network of biochemical pathways that lead to a change in the wall's compliance.

A prominent vasodilator involved in this process is Nitric Oxide (NO), the production of which, taking place in the ECs, is triggered by WSS. However, not all types of WSS can elicit a response from ECs. Many experimental observations have confirmed ECs and EGL's preferential behavior towards forward laminar flows. The EGL only reorients its structure in the presence of a flow that has a forward component (Chien, 2007). ECs release vasodilators upon prolonged exposure to laminar

^{*} Corresponding author. 800 Lancaster Ave. Department of Mechanical Engineering, Villanova University, PA, 19085, USA. E-mail address: qianhong.wu@villanova.edu (Q. Wu).

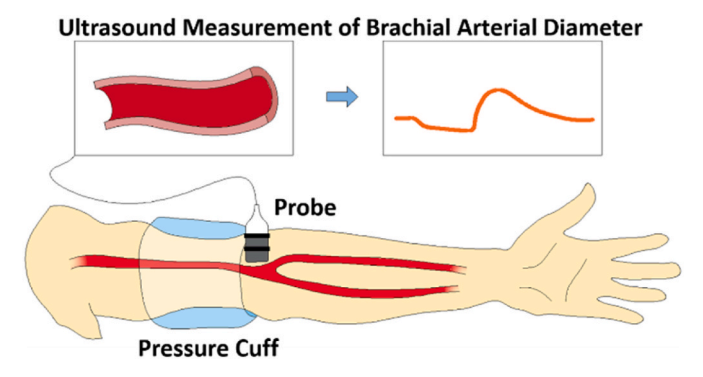


Fig. 1. Schematic of the FMD test.

flow (Nishida et al., 1992). Forward WSS magnitude has been shown to affect NO production levels (Noris et al., 1995) while upregulation of NO failed in response to a turbulent flow. Reduced blood flow, on the other hand, has been shown to attenuate vasodilation in-vivo (Kaiser et al., 1989).

The details of mechanotransduction and its mechanisms on the level of the EGL and ECs have been studied extensively (Fu and Tarbell, 2013; Haeren et al., 2016; Baeyens et al., 2014; Yao et al., 2007; Pikoula et al., 2018; Bartosch et al., 2017; Ebong et al., 2014; Zeng and Liu, 2016; Tarbell and Ebong, 2008; Tarbell and Cancel, 2016; Tarbell and Pahakis, 2006; Shi et al., 2010; Wang et al., 2006; Loth et al., 2003; Secomb et al., 2001; Thi et al., 2004). However, according to a recent comprehensive review on the subject (Weinbaum et al., 2020), this phenomenon had never been investigated on a timescale shorter than 10 min. Through the lens of physics-based modeling, and guided by the experimental observations cited above, our group was the first to tackle this limitation by modeling the arterial response during a BAFMD test (Sidnawi et al., 2020, 2021). Since mechanotransduction lies at the core of FMD, modeling its observable effects on the arterial behavior during this test can offer important insights into its short timescale operation. The model that was developed in our first study (Sidnawi et al., 2020), treated the wall as a thin elastic cylindrical shell, whose stiffness (an indicator of compliance) depends on the WSS. In its dimensionless form, the resulting equation governing the FMD response independently predicted a hallmark of mechanotransduction that was persistent in all the experimental responses, where an initially slow expansion was observed, which then picks up pace before eventually reaching a dwelling phase. The model that was presented in our second study (Sidnawi et al., 2021) was more involved. The thickness of the arterial wall was accounted for, and the diffusion time of the vasodilators throughout the wall was accommodated via the introduction of a conceptual surrogate property representing the vasodilators' local concentration. In addition to replicating the prediction of the first simplified model, this one made an intriguingly close prediction of the measured outer-to-inner diameter ratio. Each of the dimensionless parameters arising from that model has a precise physical meaning that can serve as a quantifier of arterial health. In another more recent noteworthy study that came out recently (Ma et al., 2021), the authors modeled the NO diffusion throughout the wall as it modulated the arterial response to the internal blood pressure during the recovery phase of the BAFMD test. However, unlike our two earlier models, variability across individuals was not accounted for, as the parameters governing the WSS effect on NO production, and those governing the latter's effect on arterial stiffness, were obtained from previously reported in-vitro experimental results. Also, the average NO concentration across the wall's thickness was employed as the predictor of the overall arterial stiffness, while our latest study (Sidnawi et al., 2021) accounted for the local NO effect on the space-and-time-dependent stiffness, albeit through a conceptual property as a surrogate to the local NO concentration.

A prominent limitation shared by our first two models (Sidnawi

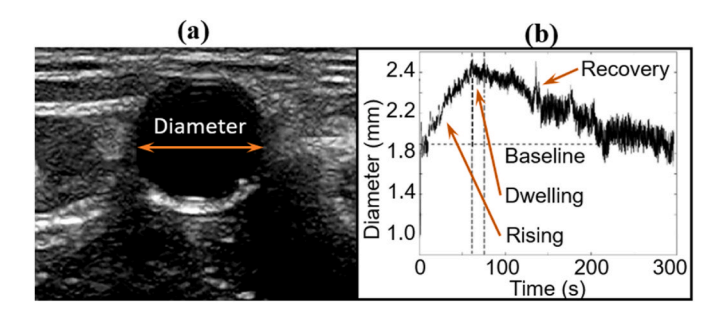


Fig. 2. (a) An image of the monitored artery. (b) The arterial response after cuff deflation. (permission for reuse is acquired)

et al., 2020, 2021) though, as well as Ma et al.'s study (Ma et al., 2021), is the lack of a viscous component contributing to the BAFMD response. The arterial wall behavior was assumed to be fully elastic. A natural question one would ask is: what is the viscous response of the blood vessel wall during the FMD process? In this study, in addition to the elastic component that was incorporated in the previous model, a viscous component will be considered. The wall's viscous parameter will also be treated as a variable quantity that is a function of both the radial location inside the wall, and the exposure time to vasodilators. Experimental BAFMD data are collected from 12 healthy volunteers, and the model is fitted to the observed response by adjusting the values of the arising parameters as needed. Key findings about the relative significance of the viscous response, are then discussed.

2. Experiment

Diameter-time response data were collected via ultrasound imaging from 12 healthy volunteers (8 males/4 females) aged 23–66, and the study was approved by the institutional review committee. The test was administered in the morning with all subjects fasting. Images were obtained using a Zonare ultrasound scanner (ZONARE Medical Systems, Bernardo, CA, USA).

An ischemic pressure cuff wrapped around a subject's upper arm was held at 250 mmHg for 5 min, while the brachial artery's diameter is being monitored (Fig. 2a). The main goal of applying pressure to the arm is to achieve complete arterial collapse, cutting off the blood flow. The pressure and duration values that are used in the current study were enough to accomplish this in all subjects. The fact that none of them had their systolic pressure anywhere near 250 mmHg when it was measured prior to each test offers a reasonable explanation as to why these values were enough. The same values were also used in the experimental protocol of a recent FMD study (Chen et al., 2019). After the artery is fully compressed, the cuff is deflated, and the diameter expansion followed by its eventual recovery to the baseline is observed (Fig. 2b). The diameter-time data were extracted after processing the images in MATLAB. The brightness contrast between the lumen and the arterial wall, which is illustrated in Fig. 2a, was the main indicator used for inferring the diameter at each frame.

As described in Fig. 2b, the arterial response features a relatively quick expansion that is followed by a brief dwelling phase before the eventual recovery to its baseline value. As in our two previous studies (Sidnawi et al., 2020, 2021), recovery will be excluded from the current model, which will be focusing on the rising and dwelling phases as they are directly prompted by the imposed sudden mechanical stimuli entailed by cuff deflation.

3. Model

The mathematical formulation, which will be detailed shortly, is rooted in the hypothesis proposed in our two previous studies (Sidnawi et al., 2020, 2021), describing a feedback loop initiated by a sudden

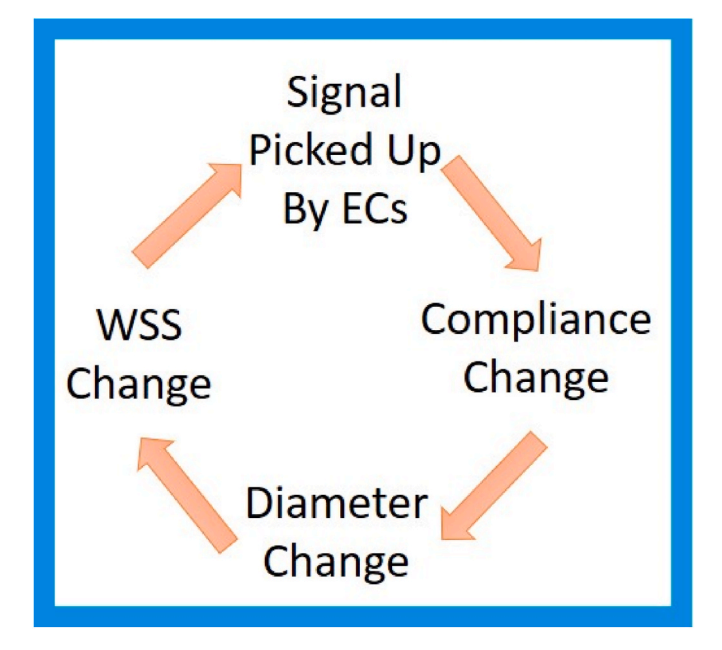


Fig. 3. The hypothesis underlying the model.

increase in WSS, which is picked up by the arterial wall's endothelial cells, thereby prompting the release of vasodilators leading to a compliance change that triggers a diameter change which in turn affects the WSS. The hypothesis is illustrated in Fig. 3.

A diffusing property, $s\left(N/m^2\right)$, which was introduced in our previous study (Sidnawi et al., 2021) as a surrogate quantity for the softening effect of the released vasodilators, will be incorporated here. The equation governing its diffusion through the wall in cylindrical coordinates is:

$$\frac{\partial s}{\partial t} = \alpha_s \left(\frac{\partial^2 s}{\partial r^2} + \frac{1}{r} \frac{\partial s}{\partial r} \right) \tag{1}$$

where t(s) is time, r (m) is the radial distance from the center, and $\alpha_s(m^2/s)$ is the diffusivity. As noted in the earlier study (Sidnawi et al., 2021), explicitly modeling the NO diffusion through the wall would be much more meaningful if in-vivo experimental data on how the wall's local mechanical properties respond to the vasodilator were available. Such a challenging experimental undertaking has never been reported before. It is important to point out that although s has the dimension of stress, it is intended as a surrogate, diffused quantity representing the transport of vasodilators throughout the arterial wall's thickness.

In addition to the elastic response, E(t), to the softening effect of s, which was the only component considered in the previous study (Sidnawi et al., 2021), the viscous response, $\eta(t)$, will also be considered here. The local values of the elastic modulus, $E_s(s)$, and viscous parameter, $\eta_s(s)$, are assumed to take on initial zero-shear maximum values, E_0 , and η_0 , respectively, and minimum values, E_∞ , and η_∞ , corresponding to $s{\to}\infty$. The subscript in $E_s(s)$ and $\eta_s(s)$ indicates that these are the values of the elastic modulus and the viscous parameter that are eventually reached in response to a sustained exposure to a softening signal of value s. $E_s(s)$ and $\eta_s(s)$ are assumed to have an exponential form given by Eq. (2).

$$E_s(s) = (E_0 - E_\infty)e^{-\beta_1 s} + E_\infty$$
 (2a)

$$\eta_s(s) = (\eta_0 - \eta_\infty)e^{-\beta_2 s} + \eta_\infty \tag{2b}$$

where β_1 (m^2/N) and β_2 (m^2/N) are characteristic properties that indicate the wall's resistance to a changing value of s; a higher value means a lower resistance for both. The exponential form assumed in Eq. (2) is not

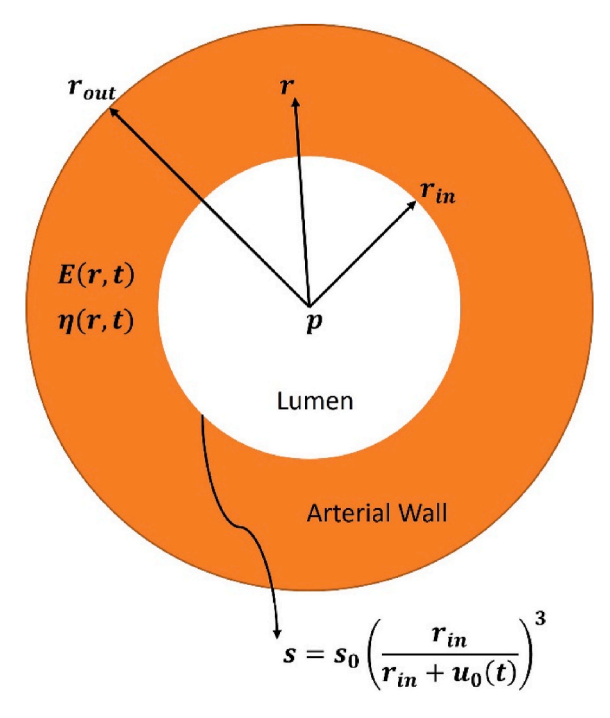


Fig. 4. A sketch describing the problem.

any more or less special than a sigmoid function or a Prony series for example, as both exhibit similar characteristics. However, in the absence of the experimental guidance alluded to after Eq. (1), it would be futile to dwell on which form is more adequate. At this stage, the fact that a change in the parameter entailed by the used exponential function can correspond to physical changes in the artery, makes that form a decent start.

The transient responses of E(t) and $\eta(t)$, to sudden step-changes in the value of s, from s_1 to s_2 , occurring at a time t_0 , are also assumed to be exponential functions of time (Eq. (3))

$$E(t) - E_s(s_2) = [E_s(s_1) - E_s(s_2)]e^{-\xi_1(t-t_0)}$$
(3a)

$$\eta(t) - \eta_s(s_2) = [\eta_s(s_1) - \eta_s(s_2)]e^{-\xi_2(t - t_0)}$$
(3b)

where ξ_1 (s^{-1}) and ξ_2 (s^{-1}) are properties of the artery that quantify its responsiveness to a changing WSS. For both, a greater value indicates a more responsive artery. From Eqs. (2) and (3), the equations governing E(t) and $\eta(t)$ in response to any continuous signal s(t) can be obtained (Eq. (4)).

$$\frac{dE}{dt} + \xi_1 E = \xi_1 E_s(s(t)) \tag{4a}$$

$$\frac{d\eta}{dt} + \xi_2 \eta = \xi_2 \, \eta_s(s(t)) \tag{4b}$$

The slow expansion observed in the rising-and-dwelling part of the FMD response makes it reasonable to assume the process as quasi-static, where the elastic and viscous parts of the response are counteracting the internal blood pressure to maintain equilibrium. Also, since an oscillatory or disturbed flow, lacking a forward component has been shown to be practically inconsequential to vasodilation stimulation (Chien, 2007; Noris et al., 1995), only the steady components of the local pressure signal, flow rate, and WSS will be accounted for. In Fig. 4, the artery is depicted as an initially unstretched cylindrical shell of inner and outer radii as r_{in} and r_{out} , respectively. At t=0, a flow rate, $q(m^3/s)$, and internal pressure $p(N/m^2)$ are introduced (corresponding to the cuff deflation). Evidently, it can still be argued that even q could change during the rising phase of the FMD response. However, absent a direct

measurement of the instantaneous flow rate that is performed in tandem with observing the arterial diameter response, an average constant value was assumed. Nevertheless, what gives us confidence in the soundness of this assumption is that it also underlaid the model in our previous work (Sidnawi et al., 2021), where only the elastic aspect of the arterial wall was considered, and where the predicted outer-to-inner diameter ratio agreed reasonably well with what was experimentally measured, in addition to reproducing the arterial behavior up to the peak diameter after cuff deflation. Since only steady components are considered, the wall shear stress, $\tau_w(N/m^2)$ would be derived from Poiseuille's parabolic solution for the velocity profile.

$$\tau_w(t) = \frac{4\mu q}{\pi R(t)^3} \tag{5}$$

where $\mu(kg/m.s)$ is the blood's dynamic viscosity, and R(t) is the inner, deformed radius. Note that $\tau_w(t)$ is $s(r_{in}, t)$. Denoting the radial displacement, and the displacement of the inner boundary, as u(r,t), and $u_0(t)$, respectively, then $R(t) = r_{in} + u_0(t)$, and Eq. (5) is recast as:

$$s(r_{in},t) = s_0 \left(\frac{r_{in}}{r_{in} + u_0(t)}\right)^3$$
 (6)

where $s_0 = \frac{4\mu q}{\pi r_n^3}$. An important distinction should be emphasized before proceeding. The property s was introduced as a surrogate property to the explicit NO concentration, [NO], which to our knowledge, was never measured in-vivo during the FMD test, if such a measurement is even possible while keeping the procedure noninvasive. s was conceived as a diffusing signal carrying the real effect of relaxing the smooth muscle cells, which is macroscopically manifested as a decrease in the effective stiffness. In our model, according to Eq. (6), s does assume the instantaneous value of the WSS, but only at the wall's inner boundary. However, the way Eq. (1) is stated (which governs the value of s beyond the inner boundary), does not, in fact, imply any specific relationship between s and [NO], and especially not a linear one. This is because based on Eq. (1), any linear relationship between s and [NO], would force the diffusivity of the signal s, α_s to be the diffusivity of NO itself. But no such

developed so far from the heart's left ventricle, making the change with respect to z ($\partial/\partial z$), in the region where FMD is observed, vanishingly small, and therefore implying that $\frac{\partial \sigma_x}{\partial z}=0$, hence rendering this shear component of the stress tensor inconsequential to radial equilibrium.

The wall's constitutive equations are:

$$\begin{bmatrix} \sigma_{rr} \\ \sigma_{\theta\theta} \end{bmatrix} = \frac{1}{1 - \nu^2} \begin{bmatrix} E & E\nu & \eta & \eta\nu \\ E\nu & E & \eta\nu & \eta \end{bmatrix} \begin{bmatrix} \varepsilon_{rr} \\ \varepsilon_{\theta\theta} \\ \dot{\varepsilon}_{rr} \\ \dot{\varepsilon}_{\theta\theta} \end{bmatrix}$$
(8)

where E is the elasticity modulus, ε is the strain tensor, and ν is the Poisson's ratio. The current study is intended as a follow-up on our previous one (Sidnawi et al., 2021), in which only the elastic component of the artery was considered. In the current work we explore the possibility of a significant viscous contribution, at least in the strict context of the FMD response. Therefore, the viscous effect elicited by the deformation rates, in contributing to the balance against the inner pressure is brought in as a component that is working in parallel with its elastic counterpart. Note how in Eq. (8), the viscous response is added to its elastic counterpart by including the effect of strain rates, $\dot{\varepsilon}_{rr}$, and $\dot{\varepsilon}_{\theta\theta}$. And since we are treating the wall material as a continuum rather than discrete, separate viscous and elastic parts, a locally homogenous material element in that continuum would have its degrees of freedom simultaneously affecting both the elastic and the viscous forces, which adds them up in response to deformation. In fact, this is simply a continuum version of the traditional Kelvin-Voigt model, which has the elastic and viscous components mounted in parallel. Without in-vivo experimental techniques that can capture the change in intrinsic mechanical properties of the wall in response to flow change during FMD, this model was deemed a good starting point. Furthermore, this further emphasizes the role of our series of studies (Sidnawi et al., 2020, 2021), including this one, in laying out a theoretical framework within which more refined models can be developed in the future as better measurement techniques and experimental protocols become available. Recognizing that $\varepsilon_{rr} = \frac{\partial u}{\partial r}$, and $\varepsilon_{\theta\theta} = \frac{u}{r}$, eqs. (7) and (8) lead to the wall's equilibrium equation:

$$\eta \frac{\partial^3 u}{\partial t \partial r^2} + \left(\frac{\partial \eta}{\partial r} + \frac{\eta}{r}\right) \frac{\partial^2 u}{\partial t \partial r} + \left(\frac{\nu}{r} \frac{\partial \eta}{\partial r} - \frac{\eta}{r^2}\right) \frac{\partial u}{\partial t} + E \frac{\partial^2 u}{\partial r^2} + \left(\frac{\partial E}{\partial r} + \frac{E}{r}\right) \frac{\partial u}{\partial r} + \left(\frac{\nu}{r} \frac{\partial E}{\partial r} - \frac{E}{r^2}\right) u = 0$$

$$\tag{9}$$

statement has been made about α_s . Still, this conceptual property proved instrumental for the successful predictions made in our earlier work (Sidnawi et al., 2021).

As the problem is axisymmetric, dependence on the angular coordinate, θ , vanishes, and the wall radial equilibrium equation reduces to:

$$\frac{\partial \sigma_{rr}}{\partial r} + \frac{1}{r} (\sigma_{rr} - \sigma_{\theta\theta}) = 0 \tag{7}$$

where σ is the stress tensor, and θ is the angular coordinate. As for the axial (z direction) equilibrium, σ_{rz} changes in the radial coordinate and does contribute to the equilibrium in the axial direction. However, σ_{rz} would not contribute to the equilibrium in the radial direction, along which the artery's expansion, which is what this study is concerned with, is taking place. Especially that the instantaneous flow field is fully

Substitute Eq. (2) in Eq. (4) to obtain the equations governing E(r,t), and n(r,t) as:

$$\frac{\partial E}{\partial t} + \xi_1 E = \xi_1 \left[(E_0 - E_\infty) e^{-\beta_1 s} - E_\infty \right]$$
 (10a)

$$\frac{\partial \eta}{\partial t} + \xi_2 \eta = \xi_2 \left[(\eta_0 - \eta_\infty) e^{-\beta_2 s} - \eta_\infty \right] \tag{10b}$$

Introducing the dimensionless variables

$$r^* = \frac{r}{r_{in}}, \ t^* = \frac{\xi_1 t}{2 \ln(10)}, \ u^* = \frac{u}{r_{in}}, \ E^* = \frac{E}{E_0}, \ \eta^* = \frac{\eta}{\eta_0}, \ s^* = \frac{s}{s_0}$$
 (11)

the system of equation governing the process can then be obtained as:

$$\frac{\Gamma}{2\ln(10)} \left[\eta^* \frac{\partial^3 u^*}{\partial t^* \partial r^{*2}} + \left(\frac{\partial \eta^*}{\partial r^*} + \frac{\eta^*}{r^*} \right) \frac{\partial^2 u^*}{\partial t^* \partial r^*} + \left(\frac{\nu}{r^*} \frac{\partial \eta^*}{\partial r^*} - \frac{\eta^*}{r^{*2}} \right) \frac{\partial u^*}{\partial t^*} \right] + E^* \frac{\partial^2 u^*}{\partial r^{*2}} + \left(\frac{\partial E^*}{\partial r^*} + \frac{E^*}{r^*} \right) \frac{\partial u^*}{\partial r^*} + \left(\frac{\nu}{r^*} \frac{\partial E^*}{\partial r^*} - \frac{E^*}{r^{*2}} \right) u^* = 0$$

$$(12a)$$

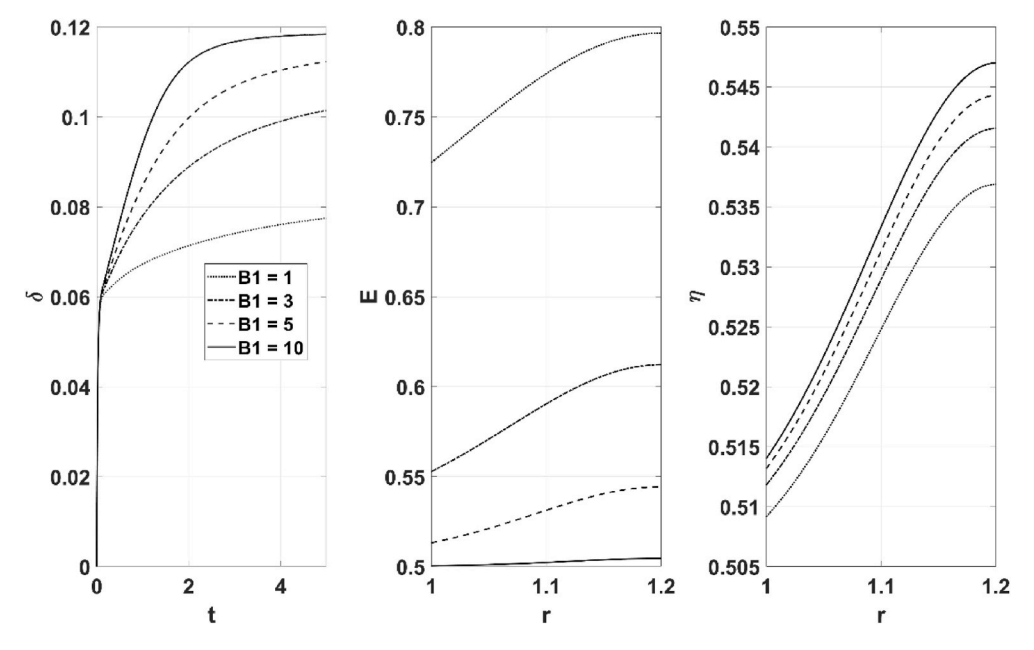


Fig. 5. δ , E, and η behavior for different values of B_1

$$\frac{\partial E^*}{\partial t^*} + 2\ln(10)E^* = 2\ln(10)\left[\left(1 - E_{min}^*\right)e^{-B_1s^*} + E_{min}^*\right]$$
 (12b)

$$\frac{\partial \eta^*}{\partial r^*} + 2\ln(10)\widehat{\xi}\eta^* = 2\ln(10)\widehat{\xi}\left[\left(1 - \eta_{min}^*\right)e^{-B_2s^*} + \eta_{min}^*\right]$$
 (12c)

$$\frac{\partial s^*}{\partial t^*} = 2 \ln(10) \gamma \left(\frac{\partial^2 s^*}{\partial r^{*2}} + \frac{1}{r^*} \frac{\partial s^*}{\partial r^*} \right)$$
 (12d)

The dimensionless parameters characterizing the response are given in Eq. (13) below.

$$\Gamma = \frac{\eta_0 \xi_1}{E_0}, \ \gamma = \frac{\alpha_s}{r_{in}^2 \xi_1}, \ B_1 = \beta_1 s_0, \ B_2 = \beta_2 s_0, \ \hat{\xi} = \frac{\xi_2}{\xi_1}, \ E_{min}^* = \frac{E_\infty}{E_0}, \ \eta_{min}^* = \frac{\eta_\infty}{E_0}, \ p^* = \frac{p}{E_0}, \ a = \frac{r_{out}}{r_{in}}$$

$$(13)$$

As explained in our previous study (Sidnawi et al., 2021), E_{min}^* is a measure of the arterial wall's sensitivity to WSS. As E_{min}^* approaches its maximum value of 1, the wall becomes increasingly indifferent to WSS. B_1 , which is related to β_1 , quantifies the wall's resistance to the softening effect of the vasodilators. The higher B_1 is, the less resistant the arterial wall becomes to softening. γ provides a measure of how active mechanotransduction is since it is directly related to the diffusivity α_s . A decreasing value of γ could therefore signal a deteriorating mechanotransduction. B_2 and η_{min}^* are the viscous counterparts of B_1 and E_{min}^* , respectively, the two latter quantities pertaining to the elastic component of the response. $\hat{\xi}$ is the viscous component's relative responsiveness to the softening signal, s, as compared to that of the elastic component. A value of $\hat{\xi}$ that is greater than 1 means that the viscous parameter, η , responds faster than the elastic modulus, E, to a changing value of s. Finally, Γ quantifies the prominence of the FMD response's viscous component, relative to its elastic counterpart. Higher values of Γ indicate a more viscous arterial wall.

Eq. (6) states the boundary condition for s at $r=r_{in}$. At the outer boundary, $r=r_{out}$, there is no further regions into which s can diffuse, thereby requiring its radial gradient there to vanish $\left. \left(\frac{\partial s}{\partial r} \right|_{r_{out}} = 0 \right)$. In dimensionless form:

$$s^*(1,t) = \left(\frac{1}{1 + u_0^*(t^*)}\right)^3 \tag{14a}$$

$$\frac{\partial s^*}{\partial r^*}(a,t) = 0 \tag{14b}$$

The stress boundary conditions, $\sigma_{rr}(r_{in},t)=-p$, and $\sigma_{rr}(r_{out},t)=0$, imply those of the dimensionless displacement, u^* , as:

$$\left[E^* \left(\frac{\partial u^*}{\partial r^*} + \nu \frac{u^*}{r^*} \right) + \frac{\Gamma}{2 \ln(10)} \left(\frac{\partial^2 u^*}{\partial t^* \partial r^*} + \frac{\nu}{r^*} \frac{\partial u^*}{\partial t^*} \right) \right] \Big|_{r^*=1} = -\left(1 - \nu^2 \right) p^* \quad (15a)$$

$$\left[E^* \left(\frac{\partial u^*}{\partial r^*} + \nu \frac{u^*}{r^*} \right) + \frac{\Gamma}{2 \ln(10)} \left(\frac{\partial^2 u^*}{\partial t^* \partial r^*} + \frac{\nu}{r^*} \frac{\partial u^*}{\partial t^*} \right) \right] \bigg|_{r^* = a} = 0$$
 (15b)

Initially, at $t^* = 0$, with no time for any diffusion or displacement to have taken place, the displacement field is 0 and the wall starts off with homogenous mechanical properties, leading to the initial conditions in Eq. (16) below.

$$u^*(r^*,0) = 0$$
 (16a)

$$E^*(r^*,0) = 1$$
 (16b)

$$\eta^*(r^*,0) = 1$$
 (16c)

$$s^*(r^*,0) = 0$$
 (16d)

The system in Eq. (12) is solved subject to Eqs. (14)–(16). The solution of Eq. (12) is obtained numerically using finite difference. The arterial wall is discretized into nodes separated by increments of size δr^* . Time is discretized into timesteps of length δt^* . The spatial derivatives in Eq. (12) are discretized based on a truncation error of $O(\delta r^{*3})$. Based on the displacement field obtained at a given timestep, Eq. (12a) is solved for the displacement u^* at each node for the next timestep. Eqs. 12 bd are then solved to obtain E^* , η^* , and s^* at each node by the next timestep, until the end of the chosen duration. To guarantee the stability of the diffusion equation's solution (Eq. (12d)), the upper bound, δt^*_{max} , of the timestep, for a given grid size, δr^* , is imposed as:

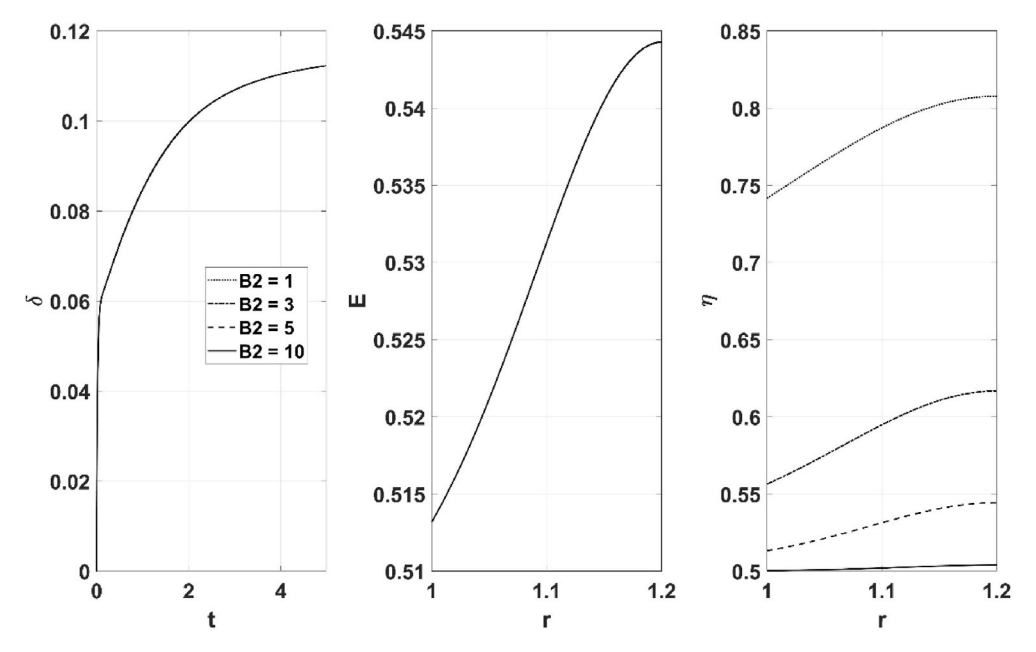


Fig. 6. δ , E, and η behavior for different values of B_2

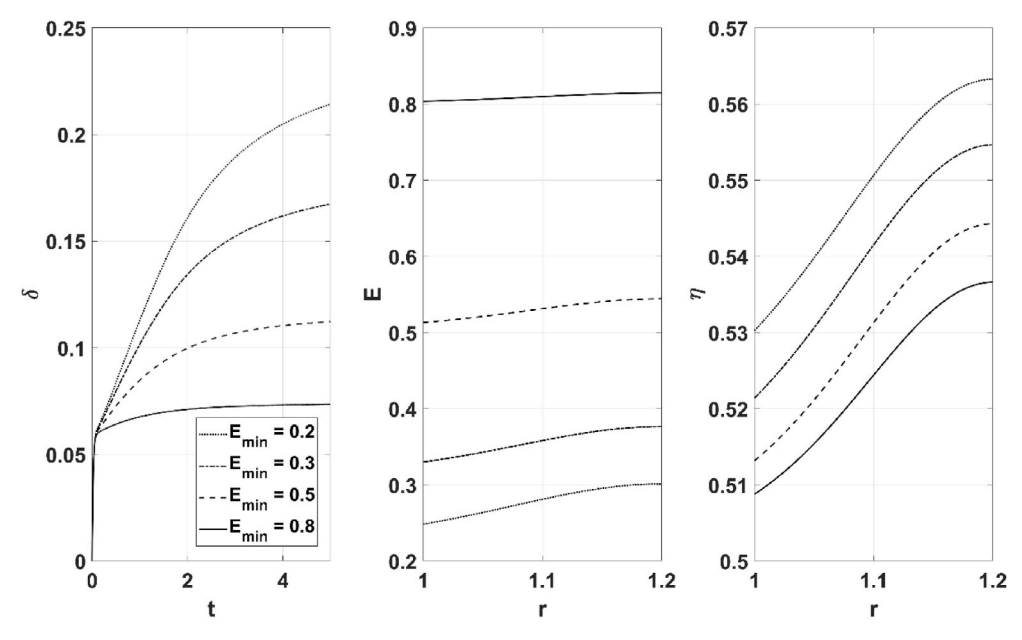


Fig. 7. δ , E, and η behavior for different values of E_{min}

$$\delta t_{max}^* = \frac{1}{4\gamma \ln(10) \left(\frac{1}{\delta r^*^2} - \frac{1}{2\delta r^* (1 + \delta r^*)}\right)}$$
(17)

This limit is due to the physical restriction that a node receiving an influx of a certain property by diffusion from an adjacent source node, cannot be given enough time between solution steps, to build up a concentration that exceeds its value at the source.

4. Results and discussion

4.1. Parametric study

To better understand the effects that key parameters in Eq. (13), after which a detailed description of those parameters' physical meaning was provided, have on the FMD response and on the wall's mechanical

properties, a parametric study will be presented. In what follows, the inner boundary's displacement, $u^*(1,t^*)$ will be denoted by δ , and the asterisk, '*', in the dimensionless quantities will be dropped for brevity. Also, the plots of E and η in this section are their profiles vs. the radial distance at the last timestep of the simulation.

The parameter \boldsymbol{B}_1 (wall's resistance to the softening effect of the vasodilators).

Fig. 5 shows the effect that changing B_1 has on the wall's response and its properties. As B_1 increases, δ increases, E decreases, and η increases. Since a higher value of B_1 indicates a lower resistance in the arterial wall's elastic modulus E to a changing WSS, the highest value of B_1 leads to the fastest elastic softening of the wall, as exhibited by E(r) for $B_1=10$. This leads to the displacement, $\delta(t)$, being the greatest for that value, and therefore, the lowest WSS, which keeps η from softening as much for $B_1=10$, as it does for lower values.

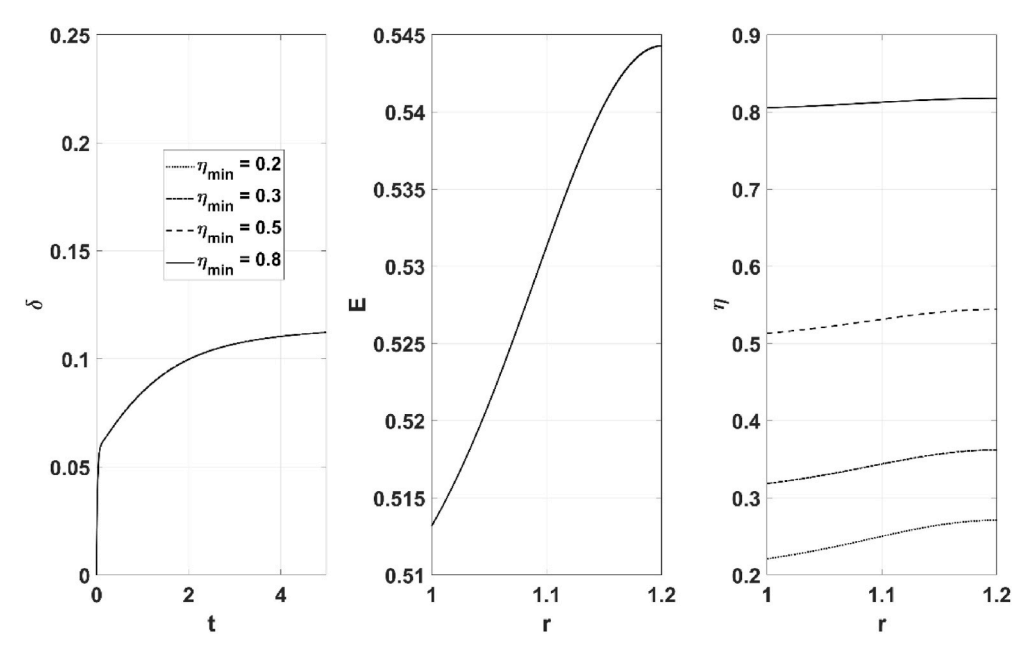


Fig. 8. δ , E, and η behavior for different values of η_{min}

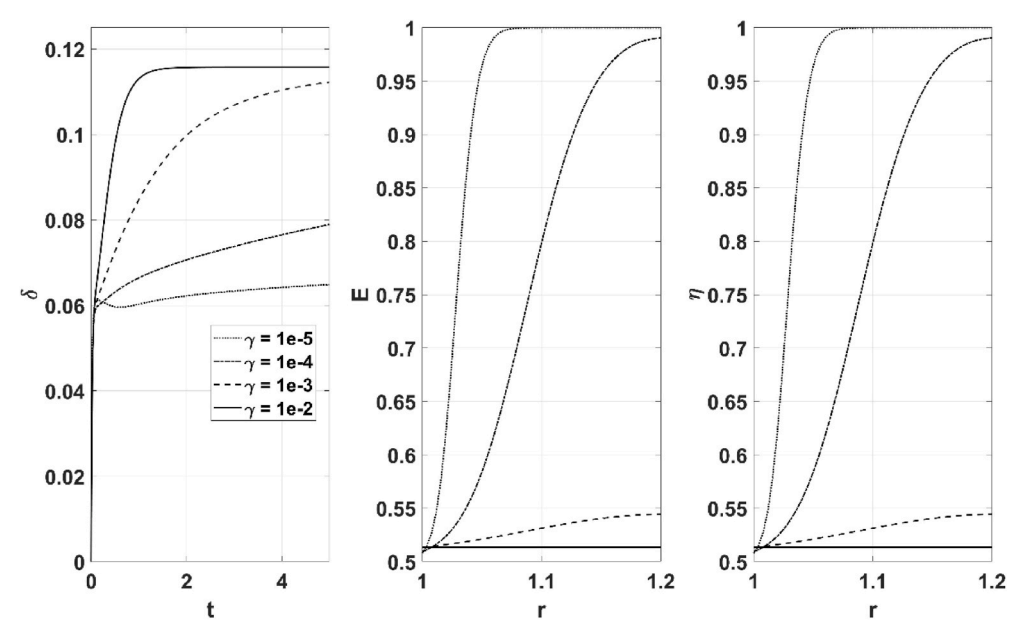


Fig. 9. δ , E, and η behavior for different values of γ

The parameter \boldsymbol{B}_2 (wall's resistance to the viscous softening effect of the vasodilators).

The effect of B_2 is shown in Fig. 6. As B_2 increases, δ and E are unaffected, and η decreases. Since B_2 is B_1 's viscous counterpart, η is the property that is affected the most by its change. The highest value of B_2 leads to the fastest viscous softening of the wall. In the absence of deformation at t=0, implying no elastic contribution to the mechanical balance against the inside pressure, it falls entirely on the viscous component of the wall's material to counteract it, therefore necessitating an initial sharp rise in δ . As deformation picks up, the elastic contribution to the balance dominates, while the viscous response is only getting softer. Since B_1 is not changing here, B_2 has virtually no effect on the primarily elastic response that comes later, and therefore $\delta(t)$ is not affected. It then follows that E, which is only determined by B_1 and $\delta(t)$ (through s^* as evident from Eq. (12b)), would not be affected

either.

The parameter E_{min} (arterial wall's sensitivity to WSS).

Fig. 7 shows the effect of changing E_{min} . As E_{min} increases, δ decreases, E increases, and η decreases. Being a measure of the wall's elastic sensitivity to WSS, when E_{min} is lowest, the wall can eventually get softest (Eq. (13)) compared to higher values of E_{min} . Therefore, at a value of 0.8, which is close to E_{min} 's upper limit of 1, the displacement $\delta(t)$ is most restricted due to the profile E(r) being highest. Since a restricted displacement maintains a higher WSS, η gets softest for the highest value of E_{min} .

The parameter η_{min} (arterial wall's viscous sensitivity to WSS).

The effect of η_{min} is shown in Fig. 8. As η_{min} increases, δ and E are unaffected, and η increases. As in the case of changing B_2 , which only pertains to the viscous softening, the dominantly elastic response that comes after the sharp rise in δ makes $\delta(t)$ and E(r) practically indifferent to changing η_{min} . With η_{min} being E_{min} 's viscous counterpart, it affects $\eta(r)$

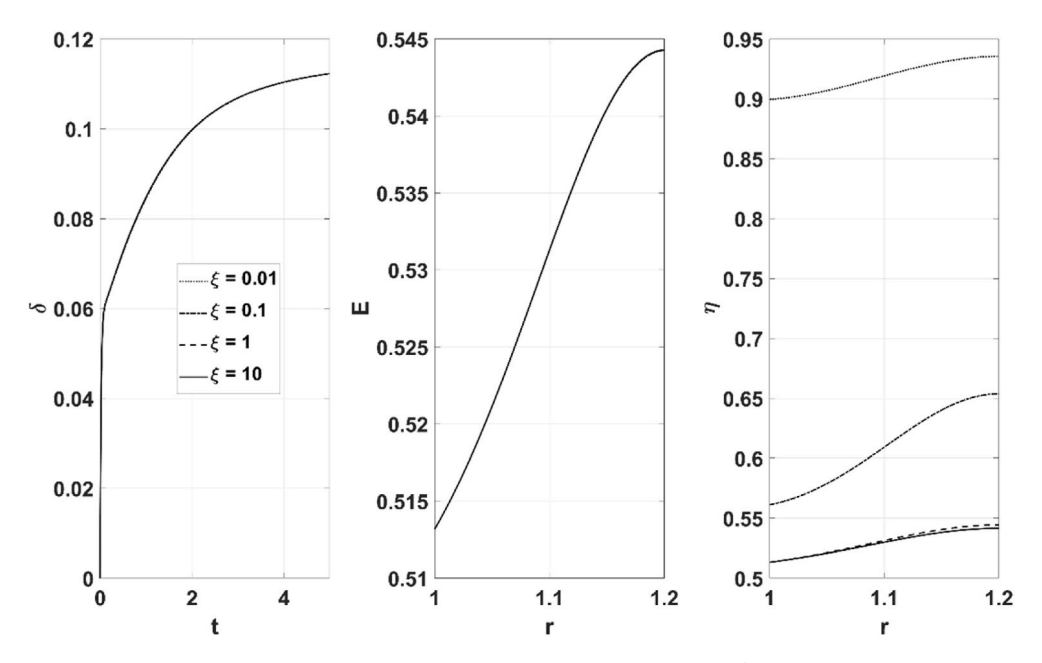


Fig. 10. δ , E, and η behavior for different values of $\hat{\xi}$

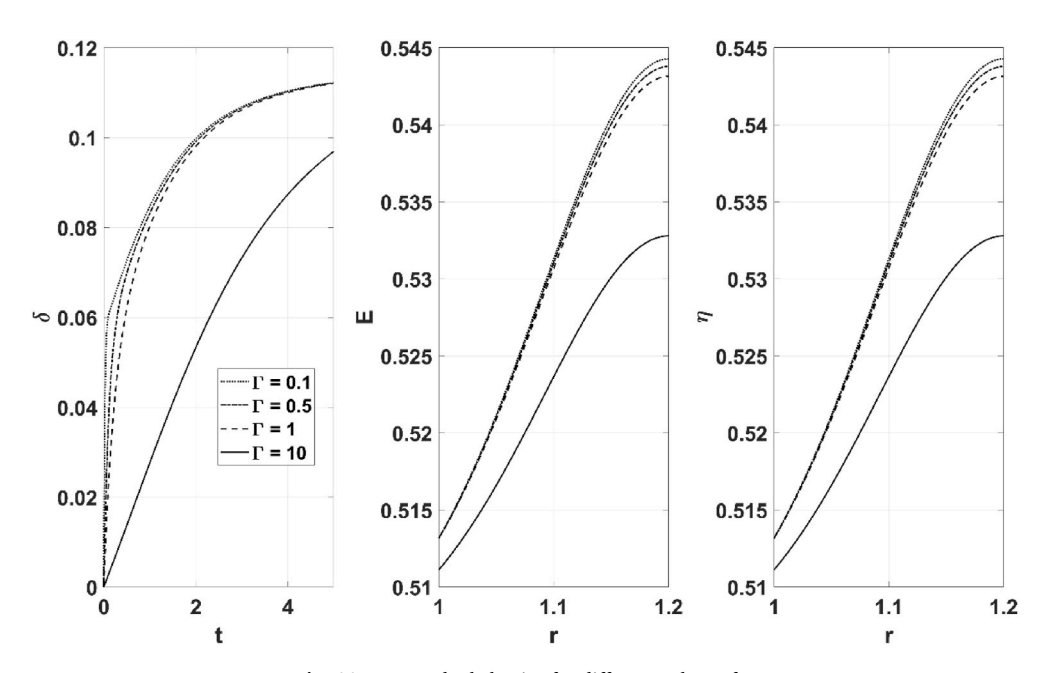


Fig. 11. δ , E, and η behavior for different values of Γ

in the same way in which E_{min} affects E(r) (Fig. 7).

The parameter γ (measure of mechanotransduction activity).

The effect of changing the mechanotransduction parameter, γ , is presented in Fig. 9. As γ increases, δ increases, and E and η decrease. Being related to the diffusivity, α_s (Eq. (13)), γ which quantifies the integrity of mechanotransduction, would lead to the fastest diffusion of the softening signal, s, through the arterial wall, when its value is highest. This is manifested by the profiles E(r) and $\eta(r)$ being softest for the highest value of γ , and consequently the deformation being highest $(\delta(t))$.

The parameter $\hat{\xi}$ (viscous-to-elastic ratio of the arterial responsiveness to the softening signal, s).

Fig. 10 shows the effect of changing $\hat{\xi}$. As $\hat{\xi}$ increases, δ and E are unaffected, and η decreases. Since $\hat{\xi}$ is η 's relative response speed to a changing value of s, as compared E's response, $\eta(r)$ is softest for the

highest value of $\hat{\xi}$. Since this parameter pertains only to the viscous response to s, $\delta(t)$, which becomes primarily elastic as explained earlier, and E(r), which is determined by $\delta(t)$ and B_1 are practically unaffected by ξ 's change.

The parameter $\boldsymbol{\Gamma}$ (prominence of the FMD response's viscous component, relative to its elastic counterpart).

Fig. 11 illustrates the effect of the viscous ratio, Γ . As Γ increases, δ , E, and η decrease. Γ indicates the relative strength of the viscous component of the response, compared to that of its elastic counterpart. Therefore, δ 's required initial rate of increase to balance the internal pressure, decreases with Γ ; hence the significantly shallower slope of $\delta(t)$ for $\Gamma=10$. Since a slower expansion maintains a longer exposure to high WSS, E(r) and $\eta(r)$ get softest for the highest value of Γ . Note however, the behavior of $\delta(t)$ for $\Gamma=0.1$. After the initial viscousdominated steep rise, the elastic-dominated response is the one that

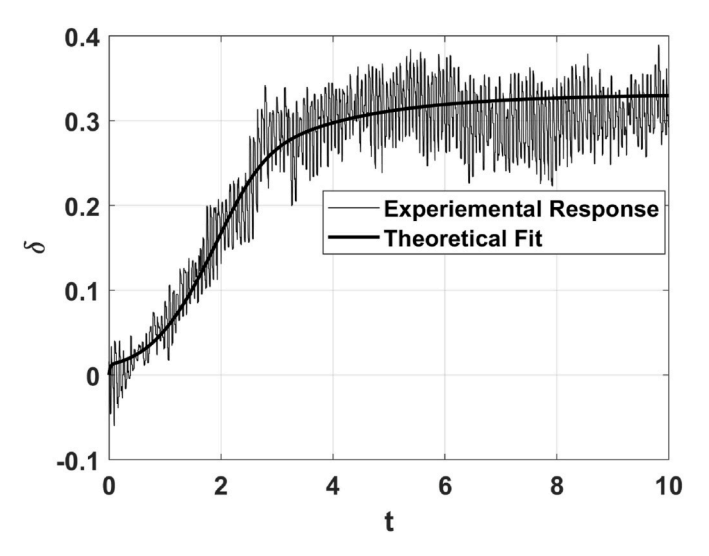


Fig. 12. The experimental and theoretical responses for one of the FMD cases.

most closely matches the observed FMD behavior, especially at the early stage, where an initial positive curvature can be seen. As will be elaborated in the next section, this is a strong hint to the fact that at least in the context of FMD, the arterial wall's elastic component is the dominant determinant of the FMD response.

4.2. Comparison with the experimental data

Through an optimization algorithm that is similar to the one used and detailed in the two previous studies (Sidnawi et al., 2020, 2021), the values of the parameters in Eq. (13), that led to a response that most closely matched the experimental response, were obtained. A representative comparison is shown in Fig. 12.

The key feature to be noted in the theoretical curve of Fig. 12, is the initial slight jump at t=0 where the viscous component of the response is supposed to be dominant. Almost immediately after this brief jump, an abrupt decrease in the slope takes place, signaling the onset of the elastic-dominated part of the response. This feature is consistent with the observations made in Fig. 11 about $\delta(t)$ for small values of Γ . Indeed,

the value of Γ corresponding to the response in Fig. 12 is found to be about 0.07. This shows that, as far as the response induced by the BAFMD test is concerned, and in the context of the current model which is a generalization that includes the purely elastic case disseminated in the previous study (Sidnawi et al., 2021), elastic forces seem to overwhelmingly dominate the response. Note that a value of Γ that is in the order of 10^2 and beyond, coupled with appropriate values for B_2 and η_{min} , can also produce a response, $\delta(t)$, that starts off slow then picks up pace due to softening, before plateauing again, which would qualitatively replicate the observed trend of its experimental counterparts. However, an arterial wall that is initially so viscous, would be difficult to reconcile with the fact that diameter fluctuations due to pressure pulsations with a period that is on a scale much smaller than that of the viscous-dominated expansion, can be observed so discernibly right from the beginning.

As evident from Eq. (12a), when $\Gamma \ll 1$, the viscous contribution to the response becomes vanishingly small, and therefore, the values of all the parameters in Eq. (13), that pertain to the viscous response, namely B_2 , $\hat{\xi}$, and η_{min} , become practically inconsequential. Hence, pursuing the values of the remaining parameters would be repeating the work reported in our previous study where only the elastic response was considered (Sidnawi et al., 2021). Fig. 13 shows the theoretical arterial response, $\delta(t)$, for different values of B_2 , $\hat{\xi}$, and η_{min} , when Γ is of the order of 10^{-2} , as was found in the matching result above. As would be expected, due to such a small value of Γ , the effect of the parameters that modulate the viscous component of the response becomes undetectable, which is manifested by the overlapping plots for all three parameters.

5. Conclusion

In this paper, the response of the brachial artery during the FMD test was analyzed in the context of a viscoelastic model that extends its purely elastic counterpart presented in the previously published study on the subject (Sidnawi et al., 2021). In addition to the parameters pertaining to the elastic response, and the one quantifying the integrity of mechanotransduction, a new set of parameters governing the viscous response, and which include the viscoelastic ratio, arose from the extended model. Experimental sets of FMD data were collected from healthy volunteers. Fitting the model's predictions for the diameter change to the experimental FMD responses resulted in values of the

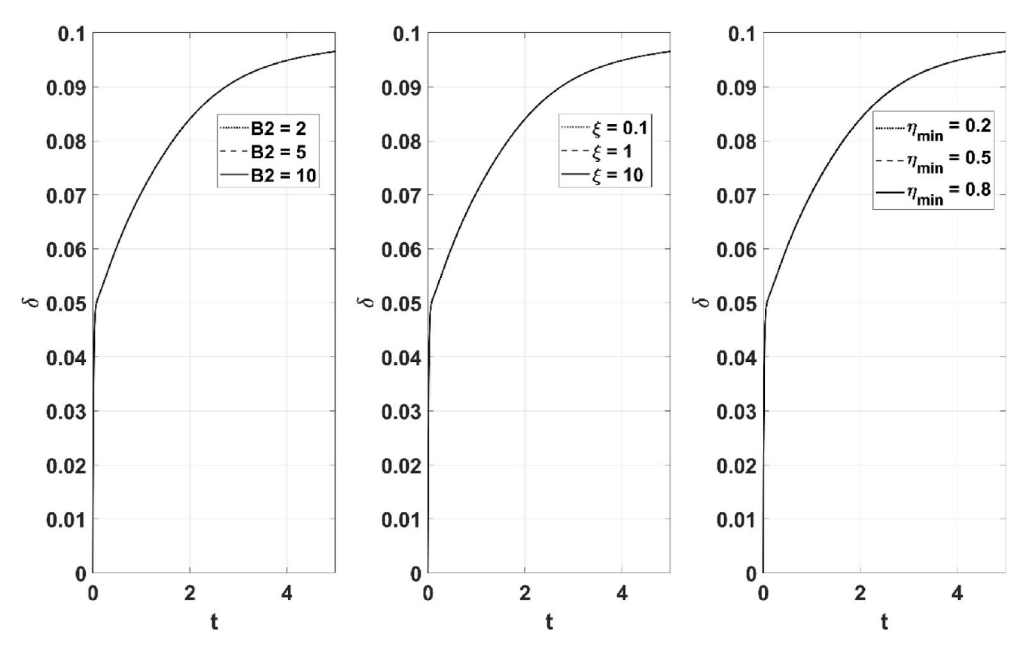


Fig. 13. The theoretical response when $\Gamma \ll 1$, for different values of B_2 , $\hat{\xi}$, and η_{min}

viscoelastic ratio that are of the order of 10^{-2} , thereby pointing to the dominance of the elastic response. Testing the sensitivity of the model to the remaining viscous parameters for such a low viscoelastic ratio showed that the theoretical response becomes virtually governed by the elastic parameters.

These findings suggest that as far as the FMD response is concerned, at the typical expansion rates that it exhibits, and in the context of the proposed theoretical tools for modeling it, which proved to possess a noticeable predictive power in our earlier work (Sidnawi et al., 2020, 2021), the arterial wall's behavior is predominantly elastic. Thus, future studies and potential clinical applications investigating cardiovascular health in light of the proposed model, can safely rely on its reduced form presented in the aforementioned precursor study (Sidnawi et al., 2021).

Our series of studies on modeling FMD (Sidnawi et al., 2020, 2021), including the current one are the first to outline a bottom-up approach that managed to reproduce the time course of the arterial response, which enabled the extraction of several physically meaningful parameters hinting at the endothelial and structural state of the arterial wall, in addition to the traditionally examined peak percent dilation (FMD%). This is far from being an assertion that specific assumptions cannot be improved upon. It is hoped that this approach, which is more of a novel theoretical framework, than a specific, final model, will spur a renewed interest and a paradigm shift in how FMD measurements are acquired (concurrent acquisition of Q(t), for example), such that more refined models can be developed.

CRediT authorship contribution statement

Bchara Sidnawi: Writing – original draft, Software, Methodology, Investigation, Formal analysis, Conceptualization. Sridhar Santhanam: Writing – review & editing, Validation, Supervision, Methodology, Conceptualization. Chandra Sehgal: Writing – review & editing, Supervision, Methodology, Investigation, Funding acquisition, Data curation. Qianhong Wu: Writing – review & editing, Validation, Supervision, Methodology, Investigation, Funding acquisition, Formal analysis, Conceptualization.

Declaration of competing interest

The authors declare that they have no known competing financial interests or personal relationships that could have appeared to influence the work reported in this paper.

Acknowledgment

This work was performed in partial fulfillment of the Villanova University Ph. D requirements for B.S., who is partially supported by the National Science Foundation's Grant No. 2003077, and 1511096. The support from the National Institute of Health, under Awards No. R21 EB005326 is also acknowledged.

References

- Baeyens, N., et al., 2014. Syndecan 4 is required for endothelial alignment in flow and atheroprotective signaling. Proc. Natl. Acad. Sci. U.S.A. 111, 17308–17313.
- Bartosch, A.M.W., Mathews, R., Tarbell, J.M., 2017. Endothelial glycocalyx-mediated nitric oxide production in response to selective AFM pulling. Biophys. J. 113, 101–108.
- Birk, G.K., et al., 2012. Brachial artery adaptation to lower limb exercise training: role of shear stress. J. Appl. Physiol. 112, 1653–1658.
- Broxterman, R.M., et al., 2019. Strong relationship between vascular function in the coronary and brachial arteries: a clinical coming of age for the updated flow-mediated dilation test? Hypertension 74, 208–215.

- Celermajer, D.S., et al., 1993. Cigarette smoking is associated with dose-related and potentially reversible impairment of endothelium-dependent dilation in healthy young adults. Circulation 88, 2149–2155.
- Chen, Z., Sultan, L.R., Schultz, S.M., Cary, T.W., Sehgal, C.M., 2019. Brachial flow-mediated dilation by continuous monitoring of arterial cross-section with ultrasound imaging. Ultrasound 27, 241–251.
- Chien, S., 2007. Mechanotransduction and endothelial cell homeostasis: the wisdom of the cell. Am. J. Physiol. Heart Circ. Physiol. 292.
- Ebong, E.E., Lopez-Quintero, S.V., Rizzo, V., Spray, D.C., Tarbell, J.M., 2014. Shear-induced endothelial NOS activation and remodeling via heparan sulfate, glypican-1, and syndecan-1. Integr. Biol. 6, 338–347.
- Fu, B.M., Tarbell, J.M., 2013. Mechano-sensing and transduction by endothelial surface glycocalyx: composition, structure, and function. Wiley Interdiscip. Rev. Syst. Biol. Med. 5, 381–390.
- Haeren, R.H.L., et al., 2016. Assessment and imaging of the cerebrovascular glycocalyx. Curr. Neurovascular Res. 13, 249—260.
- Hashimoto, M., et al., 1998. The impairment of flow-mediated vasodilatation in obese men with visceral fat accumulation. Int. J. Obes. 22, 477–484.
- Kaźmierski, M., Michalewska-Włudarczyk, A., Krzych, Ł.J., Tendera, M., 2010. Diagnostic value of flow mediated dilatation measurement for coronary artery lesions in men under 45 years of age. Cardiol. J. 17, 288–292.
- Kaiser, L., Spickard, R.C., Olivier, N.B., 1989. Heart failure depresses endotheliumdependent responses in canine femoral artery. Am. J. Physiol. Cell Physiol. 256, H962–H967.
- Loth, F., et al., 2003. Transitional flow at the venous anastomosis of an arteriovenous graft: potential activation of the ERK1/2 mechanotransduction pathway. J. Biomech. Eng. 125, 49–61.
- Ma, T., et al., 2021. Flow-mediated dilation analysis coupled with nitric oxide transport to enhance the assessment of endothelial function. J. Appl. Physiol. 131, 1–14.
- McCully, K.K., 2012. Flow-mediated dilation and cardiovascular disease. J. Appl. Physiol. 112, 1957–1958.
- Nakamura, T., et al., 2011. Endothelial vasomotor dysfunction in the brachial artery predicts the short-term development of early stage renal dysfunction in patients with coronary artery disease. Int. J. Cardiol. 148, 183–188.
- Nishida, K., et al., 1992. Molecular cloning and characterization of the constitutive bovine aortic endothelial cell nitric oxide synthase. J. Clin. Invest. 90, 2092–2096.
- Noris, M., et al., 1995. Nitric oxide synthesis by cultured endothelial cells is modulated by flow conditions. Circ. Res. 76, 536–543.
- Pikoula, M., Tessier, M.B., Woods, R.J., Ventikos, Y., 2018. Oligosaccharide model of the vascular endothelial glycocalyx in physiological flow. Microfluid. Nanofluidics 22, 1–13
- Pyke, K.E., Tschakovsky, M.E., 2005. The relationship between shear stress and flow-mediated dilatation: implications for the assessment of endothelial function. J. Physiol. 568, 357–369.
- Secomb, T.W., Hsu, R., Pries, A.R., 2001. Effect of the endothelial surface layer on transmission of fluid shear stress to endothelial cells. Biorheology 38, 143–150.
- Shi, Z.D., Abraham, G., Tarbell, J.M., 2010. Shear stress modulation of smooth muscle cell marker genes in 2-D and 3-D depends on mechanotransduction by heparan sulfate proteoglycans and ERK1/2. PLoS One 5, 1–9.
- Sidnawi, B., Chen, Z., Sehgal, C., Wu, Q., 2020. Characterization of arterial flow mediated dilation via a physics-based model. J. Mech. Behav. Biomed. Mater. 107, 103756.
- Sidnawi, B., Chen, Z., Sehgal, C., Santhanam, S., Wu, Q., 2021. On the modeling of mechanotransduction in flow-mediated dilation. J. Mech. Behav. Biomed. Mater. 120, 104606.
- Stoner, L., Sabatier, M., Edge, K., McCully, K., 2004. Relationship between blood velocity and conduit artery diameter and the effects of smoking on vascular responsiveness. J. Appl. Physiol. 96, 2139–2145.
- Tarbell, J.M., Cancel, L.M., 2016. The glycocalyx and its significance in human medicine. J. Intern. Med. 280, 97–113.
- Tarbell, J.M., Ebong, E.E., 2008. The Endothelial Glycocalyx : A Mechano-Sensor and -Transducer, vol. 1, pp. 1–6.
- Tarbell, J.M., Pahakis, M.Y., 2006. Mechanotransduction and the glycocalyx. J. Intern. Med. 259, 339–350.
- Thi, M.M., Tarbell, J.M., Weinbaum, S., Spray, D.C., 2004. The role of the glycocalyx in reorganization of the actin cytoskeleton under fluid shear stress: a 'bumper-car' model. Proc. Natl. Acad. Sci. U.S.A. 101, 16483–16488.
- Wang, Y., Schaffler, M., Weinbaum, S., 2006. A model for the role of integrins in flow induced mechanotransduction in osteocytes. J. Biomech. 39, S238.
- Weinbaum, S., Zhang, X., Han, Y., Vink, H., Cowin, S.C., 2003. Mechanotransduction and flow across the endothelial glycocalyx. Proc. Natl. Acad. Sci. U.S.A. 100, 7988–7995.
- Weinbaum, S., Tarbell, J.M., Damiano, E.R., 2007. The structure and function of the endothelial glycocalyx layer. Annu. Rev. Biomed. Eng. 9, 121–167.
- Weinbaum, S., Cancel, L.M., Fu, B.M., Tarbell, J.M., 2020. The glycocalyx and its role in vascular physiology and vascular related diseases. Cardiovasc. Eng. Technol. https:// doi.org/10.1007/s13239-020-00485-9.
- Yao, Y., Rabodzey, A., Dewey, C.F., 2007. Glycocalyx modulates the motility and proliferative response of vascular endothelium to fluid shear stress. Am. J. Physiol. Heart Circ. Physiol. 293, 1023–1030.
- Zeng, Y., Liu, J., 2016. Role of glypican-1 in endothelial NOS activation under various steady shear stress magnitudes. Exp. Cell Res. 348, 184–189.